Schulz, H.-M., Wirth, R., Schreiber, A. (2016): Nano-Crystal Formation of TiO2 Polymorphs Brookite and Anatase Due To Organic—Inorganic Rock–Fluid Interactions. - *Journal of Sedimentary Research*, *86*, 2, pp. 59—72.

DOI: http://doi.org/10.2110/jsr.2016.1

Nano-crystal formation of TiO_2 polymorphs brookite and anatase due to organic-inorganic rock-fluid interactions

Schulz, H.-M.[1*], Wirth, R.[2] & Schreiber, A.[3]

[1] Helmholtz Centre Potsdam – GFZ German Research Centre for Geosciences, Sec. 4.3 Organic Geochemistry, Telegrafenberg, D-14473 Potsdam, Germany

Tel.: +49 331 288 1789; Fax: +49 331 288 1782

E-mail: schulzhm@gfz-potsdam.de

*Corresponding author

[2] Helmholtz Centre Potsdam – GFZ German Research Centre for Geosciences, Sec. 3.3 Chemistry and Physics of Earth Materials, Telegrafenberg, D-14473 Potsdam, Germany

Tel.: +49 331 288 1371; Fax: +49 331 288 1402

E-mail: richard.wirth@gfz-potsdam.de

[3] Helmholtz Centre Potsdam – GFZ German Research Centre for Geosciences, Sec. 3.2 Geomechanics and Rheology, Telegrafenberg, D-14473 Potsdam, Germany

Tel.: +49 331 288 1372; Fax: +49 331 288 1328

E-mail: anja.schreiber@gfz-potsdam.de

ABSTRACT

The occurrence of the titania polymorphs brookite and anatase as nano-crystals in organic matter-rich sediments of different age and thermal maturity has been investigated by means of a multidisciplinary analytical approach (FIB-TEM, organic geochemistry and petrography). It was the aim of the study to analyse the formation mechanisms, fate and behaviour of the titania nano-crystals as result of organic-inorganic rock-fluid interactions.

Brookite nano-crystals have been detected in immature Mediterranean sapropels of Quaternary age, but also anatase occurs in deeper and older black shales (Furongian Alum Shale, Sweden; Devonian to Carboniferous Bakken Shale, Williston Basin, USA). Whereas anatase prevails as single crystals, brookite nano-crystals often agglomerated. Single brookite nano-crystals from Posidonia Shale (Lower Jurassic, Northern Germany) have increasing crystal diameters with increasing maturity.

Exclusively anatase nano-crystals both as single crystals or as agglomerates have been detected at oil-water contacts in oilfields, and along fractures with fluid flow enriched in dissolved organic carbon.

Titania nano-crystal precipitation, growth (and agglomeration) takes place in the pore water of micro-environments at low to high temperatures and where low pH is coupled to the occurrence of dissolved organic components. Low sedimentation rates retaining a critical geochemical environment or higher temperatures seem major controls for the precipitation of anatase and its tendency not to agglomerate.

Key words: brookite, anatase, titanium dioxide, black shale, organic carbon

INTRODUCTION

In nature titania (TiO_2) occurs mainly in form of three polymorphs: thermodynamically most stable rutile, anatase (both tetragonal), and orthorhombic brookite. Anatase and brookite are metastable, occur at low temperatures and pressures, and may directly transform to rutile without involvement of the other metastable phase (Huberty and Xu 2008). However, the reasons for the formation of the metastable polymorphs anatase and brookite in nature instead of rutile are poorly understood, especially at low temperatures (Post and Burnham 1986). One controlling factor may be the different enthalpy of the three TiO_2 polymorphs which is dependent on the specific surface area (Ranade et al. 2002). The influence of organic matter and its degradation products may be another factor.

In sedimentary basins TiO_2 nanoparticles are described from black shales which are typically rich in organic carbon (e.g., Bernard et al. 2010, Tuschel 2013). Black shales undergo complex diagenetic processes already during deposition of organic-rich mud at the sediment-water interface. Such processes take place as interactions between solids, gas phases and fluids, and the involved phases can be inorganic or organic in nature. Such interactions are widespread in sedimentary basins and also occur at great depth. In general, these complex geochemical processes take place in aqueous solutions in which pH may be a major control for the phase stability of titania nanoparticles. Very low pH, e.g., stabilizes small rutile against anatase in very acidic solutions, but greater rutile crystal size stability is independent on pH (Finnegan et al. 2007). The irreversible conversion (or mineralization) of organic carbon -or in a more general sense “organic matter”- is the driving force for such complex interrelated processes in sediments. The conversion of labile organic compounds leads to significant geochemical changes of the pore fluid such as pH, alkalinity, etc. which may control the formation of, e.g., nanometer-sized diagenetic titania. Many of such organic-inorganic interactions are known from petroleum-bearing

74 sedimentary basins (Helgeson 1993, Seewald 2003, van Berk et al. 2013). Not directly
75 transferable in this context, but comparable to sedimentary pore fluids are wastewaters.
76 Environmental studies about the behaviour of titania nanoparticles in the presence of
77 wastewater-derived organic matter indicate that TiO_2 nanoparticle strongly settle out of
78 solution in contrast to solutions with humic acids (Neale et al. 2015). In contrast, the mean
79 TiO_2 nanoparticle diameter increases in wastewater whereas it remains nearly constant in
80 humic acid.
81 To date, only few investigations focused on diagenetic TiO_2 nanoparticles to unravel
82 organic-inorganic interactions which may control brookite or anatase precipitation in
83 sediments. The study of such interactions during titania formation requires the
84 development of new paradigms to understand how these complex systems function. Up to
85 now, mostly the transition from anatase to rutile has been studies intensely (Banfield et al.
86 1993), but brookite formation and the controlling factors in sedimentary environments are
87 unknown. The phase stability field of brookite thus remains undefined. This is due to the
88 fact that reaction conditions that lead to the selective growth and nucleation of brookite are
89 relatively more restrictive, because of a small stability window compared to those required
90 to geosynthesize anatase or rutile. Moreover, the diagnostic procedures to clearly
91 determine brookite phases on nanometer-scale is often complex, needs high resolution
92 imaging techniques (such as transmission electron microscopy, TEM) and identification
93 procedures, and –at least- is often not in the focus of research projects.
94 In this manuscript we aim to answer the following questions:
95 ▪ How does organic diagenesis or diagenetic products such as CO_2, CH_4, H_2, or low
96 molecular weight organic acids (LMWOAs) control the formation of nanometer-sized
97 brookite or anatase?
98 ▪ Is brookite/anatase formation restricted to a specific content of total organic carbon

(TOC) in TOC-rich sediments? If so, do these titania nanocrystals continue to grow during burial in a sedimentary basin?

- Which geochemical conditions are needed for brookite or anatase precipitation, and which role plays aggregation in sediments?
- Is brookite/anatase formation restricted to immature black shale, or are there any other geological situations at depth which also favour such titania formation?

To start answering these questions, we firstly summarize what is known about organic-inorganic interactions in sediments which may lead to brookite or anatase formation. In this chapter, we shortly make a digression into the procedures about today´s industrial production of anatase and brookite, and summarize which physicochemical frame is required which may relate to geochemical processes. Then we will report on our results from investigations of fine-grained sediments with different age, TOC-rich and TOC-poor, thermally immature to overmature in terms of organic diagenesis, but also about brookite formation in an oil-filled reservoir sandstone and along fractures with fluid flow.

Brookite and anatase from the TiO_2 system are ideal for studies of polymorphic phase transformations because both often (co-)occur in many fine-grained sediments. Especially fine-grained sediments may have a high TOC content, and the products of organic matter degradation may trigger titania precipitation, but also have primary Ti-bearing minerals which may serve as sources for Ti-release during diagenesis.

In the laboratory the synthesis of nanobrookite can be governed by standardized laboratory conditions. It is thus important to note that the interpretation of factors, which might have controlled the formation of titania nano-crystals in sedimentary basins, is limited as geological systems are complex and have changed in geological times in terms of hydrogeochemical composition and many other parameters.

TITANIA FORMATION DUE TO ORGANIC-INORGANIC INTERACTIONS IN SEDIMENTS – A BRIEF REVIEW

Titanium is generally less mobile unless hydrogeochemical conditions below pH 2 (a value of pH < 4.5 is given by other authors) are reached (Brookins 1988). However, titanium is mobilized in the presence of organic acids, which can form chelation complexes with Ti^{4+}. In natural water titanium only exists in a fully hydrated form. Such $TiO(OH)_2$ may occur in water with pH > 2, and such hydrates can be transported in colloidal state rather than as dissolved ions (Skrabal 1995). In contrast, concentrations of purely dissolved Ti^{4+} ions generally decrease with increasing contents of total dissolved solids. However, higher Ti^{4+} concentrations in organic-rich water provide further evidence of colloidal transport. Titanium may be removed from water by flocculation of colloidal material, adsorption and scavenging by precipitation of Mn and Fe oxides (Skrabal 1995).

Aggregation of titania nanoparticles in natural waters was intensively studied. Today it is general consensus that –independent on pH- an increase in ionic strength generally results in increased aggregation, but also in higher adsorption of natural organic matter (Chen et al. 2012). In contrast, higher adsorption of natural organic matter, e.g., fluvial fulvic acids, leads to less aggregation of TiO_2 nanoparticles (Domingos et al. 2009, Keller et al. 2010). However, the adsorption intensity of humic acids on anatase nanoparticles is strongly dependent on pH of aqueous solutions. Yang et al. (2009) showed that the adsorption of humic acids strongly increases below a pH value of 5 to 6 as well as the zeta potential, and that this prevents aggregation. Furthermore, results of generic experiments in aqueous solution independent on pH showed that the smaller the titania nanoparticles the larger the aggregates. Addition of oxalic acid, a typical product of early diagenesis in TOC-rich sediments, promotes aggregation, and aggregation is higher at pH 6.5 than at pH 2 (Pettibone et al. 2008).

149 In contrast to the commonly held view of titanium immobility, there is abundant evidence
150 for dissolution of titanium-bearing phases in siliciclastic sedimentary rocks, followed by
151 the mobility and final precipitation of authigenic titania (Morad 1986; Morad and Aldahan
152 1986, 1987a, b). The role of water and dissolved organic compounds for the dissolution,
153 transport and precipitation of titania was studied within the scope of soil studies (Swaine
154 and Mitchell 1960; Fitzpatrick et al. 1978; Dumon and Vigneau 1979) and demonstrated
155 that anatase and rutile can be dissolved by organic acids such as acetic acid and oxalic
156 acid. In 1999, Cornu and co-authors reported that the Ti-bearing minerals rutile and
157 anatase are not resistant against weathering in Amazonian ferralsol at a pH value of 4.5,
158 and that there is re-precipitation of anatase. The authors concluded that Ti mobility may be
159 linked to the complexing capacity of the organic compounds found in the soil solution. In
160 general, dissolved titanium is regarded to rapidly precipitate as a hydrous oxide and in the
161 following to crystallize to anatase and rutile in soils (Fitzpatrick and Chittleborough 2002).
162 Important and with relevance to the presented results is that Ti gel-like phases in soil
163 kaolinite particles may indicate Ti mobility at mineral scale (Malengreau et al. 1995).
164 Moreover, the hydrogeochemical system and the involved processes in soil (e.g.,
165 Schroeder and Shiflet 2000; Fang et al. 2009) can thus be regarded as a first hint for a
166 process analogue about organic-inorganic interactions during diagenesis in deeper TOC-
167 bearing sediments (*cf.* Deng and Dixon 2002).
168 First process studies about organic-inorganic interactions during diagenesis and the control
169 of pore water composition on authigenic brookite and anatase formation were published by
170 Hays et al. (1994). The authors interpreted diagenetic titania precipitates as result of
171 complexation of titanium by organic ligands. In this scenario, organic acids were regarded
172 as mobilization agents followed by a subsequent precipitation due to the decay of organo-
173 titanium complexes. Furthermore, dissolved organic compounds may control the transport

and precipitation of titania at higher temperatures, e.g., by hydrocarbon-rich fluids percolating organic-rich shales (Parnell 2004). At lower temperatures, the formation of anatase nanoparticles may also take place after dissolution by organic ligands in ground water and following sol-gel-like processes leading to precipitation (Cabral et al. 2012). Complexation may thus explain titanium mobility at varying temperatures. A potential complexation candidate is orthotitanic acid, which forms under acidic conditions in modern soils (Fitzpatrick et al. 1978), but also complexes of titanium with carbonate ions or organic ligands are considered (Hays et al. 1994). Additionally, the co-occurrence of diagenetic titania with either authigenic fluorapatite or crandallite may indicate that titania solubility is enhanced by phosphate complexing (Pe-Piper et al. 2011).

Rather special settings to study titania nano-crystal formation are oilfields in which formation water and oil at elevated temperatures and pressures co-exist at oil-water contacts (OWC). However, as titanium occurs at low concentrations in oilfield waters (ppb; Collins 1975), very close sources have to be considered.

Today, technical sol-gel processes to produce titania nanomaterials at low temperatures are carried out under controlled physicochemical conditions. Several parameters may serve as important key factors for comparison with subsurface conditions to find similar controls for brookite/anatase formation, fate and behaviour in organic-rich sediments or environments. The most important chemical parameter in aqueous sol-gel experiments to produce nano-crystals of brookite or anatase is low pH. Further controls to prevent agglomeration of nano-crystals are low ionic strength and high contents of acetic acid (and others, e.g, oxalic acid, fulvic/humic acid). For details see Bhave and Lee (2007), French et al. (2009), Isley and Penn (2006, 2008), and Isley et al. (2006, 2009).

CONCEPTUAL APPROACH

Sample selection

TOC-rich fine-grained sediment samples of different thermal maturities have been selected to investigate at which diagenetic stages brookite or anatase form in the presence of reactive and soluble (and thus convertible) organic material, and how such diagenetically formed titania changes during further diagenesis. According to this concept, samples from different stratigraphic levels and thermal maturities have been selected (Tab. 1, 2). In terms of stratigraphy the samples range from Furongian (Alum Shale) to Quaternary age (Mediterranean sapropels). The thermal maturity of the investigated samples ranges from immature conditions (Mediterranean sapropels) up to gas window maturity (Toarcian Posidonia Shale, northern Germany, Hils half-graben). The samples of Posidonia Shale have different thermal maturities, ranging from pre-(early)oil conditions (R_r: 0.53%) over oil maturity (R_r: 0.88%) to the beginning of dry gas formation (R_r: 1.45%), and thus represent a natural maturation sequence.

Besides this basic sample set and the basic considerations that brookite (or anatase) forms in TOC-rich, thermally immature black shale, additional samples have been selected to investigate whether titania formation also takes place when convertible and soluble oil or gas phases are present. For this, one Wealden black shale sample (lacustrine to fluvial facies of Early Cretaceous sediments in northern Germany) and two sandstone samples from the oil-water contact (OWC) in the Siri field in the Danish North Sea (reservoir: glauconite-bearing sandstone of the Palaeocene Heimdal Formation) have been selected. Additionally, two shaly samples from the SAFOD well have been taken to investigate brookite formation along a fault with aqueous fluid flow containing hydrocarbons (Tab. 1, 2).

The selected Wealden sample is from an altered flank of a graben structure in the Lower Saxony basin where hot basinal brines circulated and an unusual high maturation was

caused in contrast to the surrounding sediments.

The two samples from the Siri field (one from the oil leg, and one from the oil-water contact, OWC) have undergone severe diagenetic changes (e.g., berthierine formation as consequence of glauconite dissolution, etc.; Mu et al. 2015) as both the oil leg and the OWC are reactive interfaces where soluble hydrocarbons are converted into carbon dioxide, methane and acetic acid.

The investigated sample from the SAFOD well G is the "2" sample from a depth of 3,194 m (Janssen et al. 2014) where temperatures of 110-115°C prevail (Lockner et al. 2011) and where methane-rich fluids occur (Erzinger et al. 2006).

Besides geological age and well depth, basic organic geochemical data are available for selected samples. These are total organic carbon (TOC) content, vitrinite reflectance (R_r, %), organic matter type, and Rock Eval data (hydrogen index HI, oxygen index OI, and Tmax; Tab. 2).

Methodology

Polished thin sections were used to prepare electron transparent TEM foils. Prior to foil preparation, meaningful areas for investigation were selected in the sections. In the following, TEM foils were prepared using the focused ion beam (FIB) technique (Wirth 2004, 2009). The investigated FIB cut TEM foils have the dimensions 15 µm×10 µm×0.150 µm.

TEM was performed in a Tecnai F20 X-Twin transmission electron microscope with an acceleration voltage of 200 kV. A Schottky field emitter was used as an elctron source. The TEM is equipped with a Gatan Tridium energy filter, a Fishione high-angle annular dark-field detector (HAADF) and an EDAX x-Ray analyser with ultrathin window. TiO_2 nanoparticles were identified by chemical composition (EDS spectra) and from diffraction

249 data. High-resolution lattice fringe images in low-indexed zone-axis orientation were
250 processed applying a fast Fourier transform (FFT) to calculate a diffraction pattern. The
251 lengths of the different vectors measured from the diffraction pattern were compared with
252 calculated hkl-spacing of brookite, anatase and rutile. Additionally, the measured angles
253 between adjacent planes were compared with the calculated angles. In those cases where
254 the observed d-spacing and the adjacent angles between the lattice planes are in good
255 agreement with calculated data of the respective structure, an unambiguous identification
256 of the TiO_2 polymorph is possible. A good agreement between the observed and calculated
257 angles between adjacent planes is given if the deviation is less than 2°.
258

259 **RESULTS**

260 All investigated samples are rich in TOC which ranges from 1.5 % (Mediterranean
261 Sapropel S1) to 16.4 % (Bakken Shale; Tab. 2). The sample set covers a wide range of
262 thermal maturity of the organic material: from immature samples such as the
263 Mediterranean sapropels to highly mature samples such as the Wealden black shale (R_r:
264 1.6%; Tab. 2).
265 In TOC-rich muds from shallow sediment depth such as the Mediterranean sapropel
266 samples of Quaternary age, brookite nanocrystals form shortly after deposition and during
267 earliest diagenesis (Fig. 1, Tab. 3). After dissolution of Ti-bearing minerals, diffusion as
268 Ti^{4+}_{aq} species, and precipitation in isolated pore water cavities, these nanocrystals retain
269 their stability during ongoing diagenesis, and remain small in size even if they agglomerate
270 (Fig. 1h). However, exemplarily continuing brookite growth during diagenesis was found
271 in the investigated sample set of the Posidonia Shale in which brookite crystal diameters
272 increase from 37 nm (R_r: 0.48%) to 80 nm (R_r: 0.88%) and finally to 150-180 nm at 1.48%
273 R_r (Fig. 2b, e, h). During increasing maturity of the Posidonia Shale, the growth of the

brookite nano-crystals is coupled to a slight decrease of the oxygen indexes OI whereas the hydrogen indexes HI strongly decrease from 617 to 83 mgHC/gTOC (Tab. 2). The decrease of the HI values indicates a loss of potential to generate hydrocarbons. However, agglomeration has not been observed in these samples (see also Tab. 3). This fate and behaviour of early formed brookite indicates the stability of these nanocrystals, but also favourable aqueous micro-environments capable of ongoing $Ti^{4+}_{(aq)}$ species generation and brookite precipitation.

Still immature, but at the transition to oil generation are the samples from the Alum Shale and the Bakken Shale. Their high HI values (221 to 518 mgHC/gTOC) and low OI values (2 to 27 $mgCO_2$/gTOC) point to marine organic matter which is still immature (Tmax: 413-427 °C). Exclusively brookite (only in one case anatase) with crystal diameters of 150-220 nm (Fig. 3h) has been detected in the Bakken Shale, partly in agglomerated form with single crystal diameters of less than 20 nm (Fig. 3b, Tab. 3). In contrast, both brookite and anatase randomly occur in the Furongian to early Ordovician Alum Shale from southern Sweden (Fig. 4). Obviously, anatase occurs as idiomorphic single crystals (Fig. 4b, h), whereas brookite agglomerates are composed of single crystals with diameters of 50-100 nm (Fig. 4e). This difference in the titania polymorph type may be explained by the sedimentation rate which was extremely low for the Alum Shale (Schulz et al. 2015), and which kept anatase stable against transformation into brookite. Hence, if transformed to brookite, agglomeration took place.

Special environments where exclusively anatase forms are faults with hydrocarbon-bearing fluid flow and oil-water contacts. The peculiar growth of large anatase crystals (ca. 1.2 µm in diameter) in the Wealden sediments and the included nitrogen gas in inclusions (Fig. 5d, e) may be explained by the special formation environment. Ahmad et al. (2012) found that anatase nanocrystals from sol−gel experiments preferentially adsorb gaseous nitrogen due

299 to the acid character of anatase surfaces. In contrast, anatase agglomerates prevail at the
300 SAFOD fault (Fig. 5a, b). These agglomerates are composed of single anatase crystals of
301 less than 40 nm in size.
302 Oil-water contacts represent reactive interfaces in petroleum reservoirs where low
303 molecular hydrocarbons from the overlying oil leg are being dissolved and converted –via
304 anaerobic hydrocarbon degradation- into methane, carbon dioxide, acetic acid and
305 molecular hydrogen (see review about such processes in van Berk et al. 2013). Such
306 processes cause low pH of the aqueous phase which is rich in dissolved organic
307 compounds, and thus represent suitable environments for dissolution of Ti-bearing
308 minerals such as rutile (Fig. 6a, b). Exclusively anatase has been found in such an
309 environment of the Siri oilfield either as single crystals or as agglomerates. Single anatase
310 crystals can have diameters of around 200 nm (Fig. 6e) whereas the individual crystals of
311 the agglomerates are less than 50 nm in diameter (Fig. 6d). The agglomerates are similar in
312 diameter as found at the SAFOD fault.
313

314 **INTERPRETATIONS**

315 The results indicate that brookite and anatase precipitation requires specific
316 hydrogeochemical conditions which are already established during early diagenesis in
317 TOC-rich muds. These are low pore water pH caused by the release of diagenetic acids
318 such as acetic acid or oxalic acid from the organic material leading to a sufficient supply of
319 dissolved $Ti^{4+}_{(aq)}$ species from dissolution of titanium-bearing minerals. Such acids which
320 may control dissolution of Ti-bearing primary minerals (e.g., ilmenite, rutile, titanite, etc.)
321 are also applied in sol-gel experiments to keep pH low.
322 Many of the described nanocrystals occur as individual grains, but also aggregates mainly
323 composed of brookite nanocrystals have been found. Aggregation of firstly formed smaller

crystals is reported from hydrogeochemical conditions with low contents of dissolved organic compounds whereas aggregation in natural waters is prevented by NOM (naturally occurring organic matter). The results allow no systematic interpretation on how aggregation is controlled in the investigated sample material. Moreover, also high total dissolved solid (TDS) concentrations favour aggregation.

It is obvious that especially brookite nanocrystal growth is contingent upon low pH and low temperatures of the aqueous phase in which reactions take place. As most of the samples are from marine depositional environments, the formation water during early diagenesis is still high in total dissolved solids as it is original seawater. Coupled to low pH, aggregation of nanocrystals with similar size takes place. However, similar aggregates composed of anatase nanocrystals have not been found in the investigated black shale samples.

Acidic pore water conditions would be buffered in the presence of carbonate such as calcite which occurs in all investigated Posidonia Shale samples. As a consequence, dissolution and precipitation of titania would thus not be possible. However, brookite/anatase occur in two different environments in shale, either in open pore space (e.g., reservoir sandstone in Fig. 6) or in black shales predominantly in “closed” micro-environments, e.g., in clay minerals or mica. However, acidic and corrosive pore water characteristics may develop in both environments. According to this, micro-environments similar to those in black shales may develop in carbonate-bearing sediments and may enable localized titania precipitation.

Moreover, precipitation of brookite or anatase nanocrystals is not limited to black shale environments. As the hydrogeochemical properties of the aqueous phase are the actual control on brookite/anatase nanocrystal formation, titania may form in all other environments with similar characteristics. Finally it is the control by acid release during

early diagenesis of TOC-rich mud or in soil profiles, but also by oil degradation at OWCs or in the oil leg. In general, nucleating anatase grains are characterized by lower enthalpy (< 8 kJ/mol) compared to brookite (>10 kJ/mol; Fig. 8). During growth, the decrease of enthalpy is lower for anatase than for brookite, and at surface areas of around 4,000 m^2/mol brookite is lower in enthalpy. According to this, first formed nuclei should be tetragonal anatase which becomes unstable during growth in comparison to the orthorhombic brookite structure. Rapid crystallization, on the one hand, would thus favour the nucleation and persistence of anatase. Slow growth, on the other hand, would enable transformations into metastable brookite which would finally transform into the stable rutile polymorph (Benning and Waychunas 2008). As organic-rich mud undergoes rapid geochemical changes shortly after deposition (from oxic pore water conditions over sulphate reduction to methanogenesis), the anatase preserving conditions may rapidly change and may lead to transformation into brookite whereas similar pore water conditions at greater depth may establish over longer periods leading to conditions suitable for anatase stability and growth. Such stable pore water conditions may also explain the occurrence of predominantly anatase in the Alum Shale which was deposited over a time span of 20 Ma under similar conditions.

Density functional theory calculations performed by Li et al. (2008) showed that brookite surfaces may adsorb higher contents of formic acid in contrast to anatase. Dissolved formic acid is – besides dissolved acetic acid and oxalic acid- one of the major low-molecular weight organic acids (LMWOAs) which are generated during earliest diagenesis at shallow sediment depth (e.g., Xiao et al. 2009, 2010). However, adsorption of LMWOAs on titania nanoparticles is controlled by pH of aqueous solutions. Humic acids, e.g., are preferentially adsorbed at pH lower than 5 whereas adsorption decreases at pH higher than 5. In conclusion, brookite crystallization during early diagenesis is controlled by low pH when

374 organic acids are preferentially adsorbed.

375 In the investigated black shales brookite predominates over anatase. Brookite was found
376 either as single crystals (mainly as platy crystals, partly with thickness fringes due to
377 diffraction contrasts) or as aggregates. In general, a high ionic strength of an aqueous
378 solutions promotes titania nanocrystal aggregation (Domingos et al. 2009; French et al.
379 2009). Samples with brookite aggregates have been deposited in marine environments
380 (Mediterranean sapropels, Bakken Shale, and Alum Shale), and high ionic strength of the
381 sediment pore water can be assumed. Instead, agglomeration was not observed in the
382 Posidonia Shale which is also marine in origin. The reasons why the hydrogeochemical
383 characteristics of pore water in the Posidonia Shale during early diagenesis, but also later,
384 did not lead to agglomerates, are difficult to evaluate. It is the complex interplay of
385 multiple factors such as ionic strength, pH and resulting acid adsorption which controlled
386 whether nanocrystals agglomerate or not.

387

388 **CONCLUSIONS**

389 Brookite and anatase nano-crystals form in hydrogeochemical environments at low pH,
390 with mainly brookite already at sediment temperatures of less than 10 degrees Celsius
391 during early diagenesis. The preferred precipitation of brookite refers to the release of
392 diagenetic products such as CO_2, CH_4, H_2, LMWOAs or the early diagenetic formation of
393 humic/fulvic acids. Besides these formation controls the ionic strength of the aqueous
394 solution modifies the agglomeration tendency. Such conditions are strongly coupled on
395 available soluble organic matter, and occur in black shales with TOC values over a wide
396 range (1.5 to 16.4 wt.% TOC). After the initial precipitation of brookite nano-crystals, their
397 growth may continue during further burial provided that the hydrogeochemical conditions
398 remain stable.

In other TOC-rich environments with higher thermal maturities and high present-day temperatures (more than 60 degrees Celsius) according the prevailing burial depth, exclusively anatase forms independent on lithology such as in sandstone reservoirs in oilfields or in permeable zones in shale with fluid flow. The predominance of anatase along faults and at oil-water contacts at higher temperatures additionally reflects stable hydrogeochemical conditions in contrast to changing conditions during early diagenesis.

The formation of predominantly brookite in black shale is furthermore dependent on isolated micro-environments in which acidic and corrosive conditions may lead to dissolution of titanium-bearing minerals. Dissolved $Ti^{(4+)}_{aq}$ species in pore waters as a source for the observed titania precipitations can be due to the occurrence of rutile, ilmenite, titanite, etc. Such micro-environments can exclusively develop in isolated, water-wet cavities of impermeable TOC-rich clayey sediments during early diagenesis.

ACKNOWLEDGEMENTS

The authors are grateful to Jürgen Möbius (Hamburg, Germany), Rolando di Primio (Oslo, Norway), Johan Byskov Svendsen and Niels. H. Schovsbo (both Copenhagen, Denmark), and Christoph Janssen (Potsdam, Germany) to providing material for investigations.

REFERENCES

Ahmad, M.A., Prelot, B., Razafitianamaharavo, A., Douillard, J.M., Zajac, J., Dufour, F., Durupthy, O., Chaneac, C., and Villiéras, F., 2012, Influence of Morphology and Crystallinity on Surface Reactivity of Nanosized Anatase TiO2 Studied by Adsorption Techniques. 1. The Use of Gaseous Molecular Probes: J. Phys. Chem. C, v. 116, p. 24596−24606.

Banfield, J.F., Bischoff, B.L., and Anderson, M.A., 1993, TiO2 accessory minerals: coarsening, and transformation kinetics in pure and doped synthetic nanocrystalline materials: Chemical Geology, v. 110, p. 211-231.

Benning, L.G., and Waychunas, G.A., 2008, Nucleation, Growth, and Aggregation of Mineral Phases: Mechanisms and Kinetic Controls, in Brantley, S.L., Kubicki, J.D. and White, A.F., eds., Kinetics of Water-Rock Interaction. Springer New York. p. 259-333.

Bernard, S., Horsfield, B., Schulz, H.-M., Schreiber, A., Wirth, R., Vu, T. T. A., Perssen, F., Könitzer, S., Volk, H., and Sherwood N., 2012, Multi-scale detection of organic and inorganic signatures provides insights into gas shale properties and evolution: Chemie der Erde-Geochemistry, v. 70, p. 119-133.

Bhave, R.C., and Lee, B.I., 2007, Experimental variables in the synthesis of brookite phase TiO2 nanoparticles: Materials Science and Engineering, v. A 467, p. 146–149.

Brookins, D.G., 1988, Eh-pH Diagrams for geochemistry. Springer-Verlag, New York.

Cabral, A.R., Reith, F., Lehmann, B., Brugger, J., Meinhold, M., Tupinambá, M., and Kwitko-Ribeiro R., 2012, Anatase nanoparticles on supergene platinum–palladium aggregates from Brazil: Titanium mobility in natural waters: Chemical Geology, v. 334, p. 182–188.

Chen, G., Liu, X., and Su, C., 2012, Distinct Effects of Humic Acid on Transport and Retention of TiO2 Rutile Nanoparticles in Saturated Sand Columns: Environ. Sci.

442 Technol., v. 46, p. 7142−7150.
443 Collins, G., 1975, Geochemistry of oilfield waters. Developments in Petroleum Science, v.
444 1. Elsevier, Amsterdam. 495 p.
445 Cornu, S., Lucas, Y., Lebon, E., Ambrosi, J.P., Luizáo, F., Rouiller, J., Bonnay, M., and
446 Neal, C., 1999, Evidence of titanium mobility in soil profiles, Manaus, central Amazonia:
447 Geoderma, v. 91, p. 281–295.
448 Deng, Y., and Dixon, J.B., 2002, Soil Organic Matter and Organic-Mineral Interactions, in
449 Soil Science Society of America, ed., Soil Mineralogy with Environmental Applications,
450 SSSA Book Series 7, p. 69-107.
451 Domingos, R.F., Tufenkji, N., and Wilkinson, K.J., 2009, Aggregation of Titanium
452 Dioxide Nanoparticles: Role of a Fulvic Acid: Environ. Sci. Technol., v. 43 (5), p. 1282–
453 1286.
454 Dumon, J.C., and Vigneaux, M., 1979, Evidence for some mobility of titanium in podzols
455 and under laboratory conditions as a result of the action of organic agents: Phys. Chem.
456 Earth, v. 11, p. 331-337.
457 Erzinger, J., Wiersberg, T., and Zimmer, M., 2006, Real-time mud gas logging and
458 sampling during drilling: Geofluids, v. 6, p. 225–233.
459 Fang, J., Shan, X., Wen, B., Lin, J., and Owens, G., 2009, Stability of titania nanoparticles
460 in soil suspensions and transport in saturated homogeneous soil columns: Environmental
461 Pollution, v. 157, p. 1101–1109.
462 Finnegan, M.P., Zhang, H., and Banfield, J.F., 2007, Phase Stability and Transformation in
463 Titania Nanoparticles in Aqueous Solutions Dominated by Surface Energy: J. Phys.
464 Chem., v. C 111(5), p. 1962–1968.
465 Fitzpatrick, R.W., Le Roux, J., and Schwetmann, U., 1978, Amorphous and Crystalline
466 Titanium and Iron-Titanium Oxides in Synthetic Preparations, at near Ambient Conditions,

467 and in Soil Clays: Clays and Clay Minerals, v. 26(3), p. 189-201.
468 Fitzpatrick, R.W., and Chittleborough, D.J., 2002, Titanium and Zirconium Minerals, in
469 Soil Science Society of America, ed., Soil Mineralogy with Environmental Applications,
470 SSSA Book Series 7, p. 667-690.
471 French, R.A., Jacobson, A.R., Kim, B., Isley, S.L., Penn, R.L., and Baveye, P.C., 2009,
472 Influence of ionic strength, pH, and cation valence on aggregation kinetics of titanium
473 dioxide nanoparticles: Environ. Sci. Technol., v. 43, p. 1354–1359.
474 Hays, P.D., James, W.D., and Tieh, T.T., 1994, The role of NAA in studies of organic
475 diagenesis of rocks: Journal of Radioanalytical and Nuclear Chemistry, v. 180(1), p. 15-23.
476 Helgeson, H.C., Knox, A.M., Owens, C.E., and Shock, E.L., 1993, Petroleum, oil field
477 waters, and authigenic mineral assemblages: Are they in metastable equilibrium in
478 hydrocarbon reservoirs?: Geochimica et Cosmochimica Acta, v. 57, p. 3295–3339.
479 Huberty, J., and Xu, H., 2008, Kinetics study on phase transformation from titania
480 polymorph brookite to rutile: Journal of Solid State Chemistry, v. 181, p. 508–514.
481 Isley, S.L., and Penn, L.R., 2006, Relative brookite and anatase content in sol-gel-
482 synthesized titanium dioxide nanoparticles: Journal of Physical Chemistry B, v. 110(31), p.
483 15134-15139.
484 Isley, S.L., Anderson, E.R., and Penn, R.L., 2006, Influence of ionic strength on brookite
485 content in sol-gel synthesized titania before and after hydrothermal aging: ECS
486 Transactions, v. 3(9), p. 37-46.
487 Isley, S.L., and Penn, L.R., 2008, Titanium Dioxide Nanoparticles: Effect of Sol−Gel pH
488 on Phase Composition, Particle Size, and Particle Growth Mechanism: Journal of Physical
489 Chemistry C, v. 112(12), p. 4469-4474.
490 Isley, S.L., Jordan, D.S., and Penn, L.R., 2009, Titanium dioxide nanoparticles: Impact of
491 increasing ionic strength during synthesis, reflux, and hydrothermal aging: Materials

492 Research Bulletin, v. 44(1), p. 119-125.
493 Janssen, C., Wirth, R., Wenk, H.-R., Morales, L., Naumann, R., Kienast, M., and Dresen,
494 G., 2014, Faulting processes in active faults – Evidences from TCDP and SAFOD drill
495 core samples: Journal of Structural Geology, v. 65, p. 100–116.
496 Keller, A.A., Wang, H., Zhou, D., Lenihan, H. S., Cherr, G., Cardinale, B.J., Miller, R.,
497 and Ji, Z., 2010, Stability and Aggregation of Metal Oxide Nanoparticles in Natural
498 Aqueous Matrices: Environ. Sci. Technol., v. 44 (6), p. 1962–1967.
499 Kuhn, P., Di Primio, R., and Horsfield, B., 2010, Bulk composition and phase behaviour of
500 petroleum sourced by the Bakken Formation of the Williston Basin, in Geological Society,
501 London, Petroleum Geology Conference series 2010, v. 7, p. 1065-1077.
502 Li, W.-K., Gong, X.-Q., Lu, G., and Selloni, A., 2008, Different Reactivities of TiO2
503 Polymorphs: Comparative DFT Calculations of Water and Formic Acid Adsorption at
504 Anatase and Brookite TiO2 Surfaces: J. Phys. Chem., v. C 112 (17), p. 6594–6596.
505 Malengreau, N., Muller, J.P., and Calas, G., 1995, Spectroscopic approach for
506 investigating the status and mobility of Ti in kaolinitic materials: Clays Clay Miner., v. 43,
507 p. 615-621.
508 Morad, S., 1986, Pyrite-chlorite and pyrite-biotite relations in sandstones: Sedimentary
509 Geology, v. 49, p. 177-192.
510 Morad, S., and Aldahan, A. A., 1986, Alteration of detrital Fe-Ti oxides in sedimentary
511 rocks: Geological Society of America Bulletin, v. 97, p. 567-578.
512 Morad, S., and Aldahan, A.A., 1987a, Diagenetic replacement of feldspars by titanium
513 oxides in sandstones: Sedimentary Geology, v. 51, p. 147-153.
514 Morad, S., and Aldahan, A.A., 1987b, Diagenetic chloritization of feldspars in sandstones:
515 Sedimentary Geology, v. 51, p. 155-164.
516 Mu, N., Schulz, H.-M., Fu, Y., Wirth, R., Rhede, D., and van Berk, W., 2015, Berthierine

formation in an oil reservoir as result of fluid-rock interactions: Part I. Characterization: Marine and Petroleum Geology, v. 65, p. 302-316.

Navrotsky, A., 2004, Energetic clues to pathways to biomineralization: Precursors, clusters, and nanoparticles: Proc. Natl. Acad. Sci. USA, v. 101, p. 12096–12101.

Neale, P.A., Jämting, Å.K., O'Malley, E., Herrmann, J., and Escher, B.I., 2015, Behaviour of titanium dioxide and zinc oxide nanoparticles in the presence of wastewater-derived organic matter and implications for algal toxicity: Environmental Science: Nano, v. 2, 86-93.

Parnell, J., 2004, Titanium mobilization by hydrocarbon fluids related to sill intrusion in a sedimentary sequence, Scotland: Ore Geology Reviews, v. 24, p. 155–167.

Pe-Piper, G., Karim, A., and Piper, D.J.W., 2011, Authigenesis of Titania Minerals and the Mobility of Ti: New Evidence From Pro-Deltaic Sandstones, Cretaceous Scotian Basin, Canada: Journal of Sedimentary Research, v. 81, p. 762–773.

Pettibone, J.M., Cwiertny, D.M., Scherer, M., and Grassian, V.H., 2008, Adsorption of Organic Acids on TiO2 Nanoparticles: Effects of pH, Nanoparticle Size, and Nanoparticle Aggregation: Langmuir, v. 24, p. 6659-6667.

Post, J.E., and Burnham, C.W., 1986, Ionic modeling of mineral structures and energies in the electron gas appropximation: TiO2 polymorphs, quartz, forsterite, diopside: American Mineralogist, v. 71, p. 1142–1150.

Ranade, M.R., Navrotsky, A., Zhang, H. Z., Banfield, J.F., Elder, S.H., Zaban, A., Borse, P.H., Kulkarni, S.K., Doran, G.S., and Whitfield, H.J., 2002, Energetics of nanocrystalline TiO2: PNAS, v. 99(suppl. 2), p. 6476–6481.

Schroeder, P.A., and Shiflet, J., 2000, Ti-Bearing Phases in the Huber Formation, an East Georgia Kaolin Deposit: Clays and Clay Minerals, v. 48(2), p. 151–158.

Schulz, H.-M., Sachsenhofer, R.F., Bechtel, A., Polesny, H., and Wagner, L., 2002, The

origin of hydrocarbon source rocks in the Austrian Molasse Basin (Eocene–Oligocene transition): Marine and Petroleum Geology, v. 19(6), p. 683–709.

Schulz, H.-M., Biermann, S., van Berk, W., Krüger, M., Straaten, N., Bechtel, A., Wirth, R., Lüders, V., Schovsbo, N.H., and Crabtree, S., 2015, From shale oil to biogenic shale gas: retracing organic-inorganic interactions in the Alum Shale (Furongian-Lower Ordovician) in southern Sweden: AAPG Bulletin, v. 99(5), p. 927-956.

Seewald, J.S., 2003, Organic–inorganic interactions in petroleum-producing sedimentary basins: Nature, v. 426, p. 327–333.

Skrabal, S.A., 1995, Distributions of dissolved titanium in Chesapeake Bay and the Amazon River Estuary: Geochimica et Cosmochimica Acta, v. 59(12), p. 2449–2458.

Swaine, D.J., and Mitchell, R.L., 1960, Trace-element distribution in soil profiles: Journal of Soil Science, v. 11(2), p. 347–368.

Tuschel, D., 2013, Raman spectroscopy of oil shale: Spectroscopy, v. 28(3), 5 p. www.spectroscopyonline.com

van Berk, W., Schulz, H.-M., and Fu, Y., 2013, Controls on CO2 fate and behavior in the Gullfaks oilfield (Norway): how hydrogeochemical modeling can help to decipher organic-inorganic interactions: AAPG Bulletin, v. 97(12), p. 253–262.

Wirth, R., 2004, A novel technology for advanced application of micro- and nanoanalysis in geosciences and applied mineralogy: Eur. J. Mineral., v. 16 (6), p. 863–876.

Wirth, R., 2009, Focused Ion Beam (FIB) combined with SEM and TEM: advanced analytical tools for studies of chemical composition, microstructure and crystal structure in geomaterials on a nanometre scale: Chem. Geol., v. 261 (3–4), p. 217–229.

Xiao, M., Wu, F., Liao, H., Li, W., Lee, X., and Huang, R., 2009, Vertical profiles of low molecular weight organic acids in sediment porewaters of six Chinese lakes: Journal of

567 Hydrology, v. 365, p. 37-45.
568 Xiao, M., Wu, F., Liao, H., Li, W., Lee, X., and Huang, R., 2010, Characteristics and
569 distribution of low molecular weight organic acids in the sediment porewaters in Bosten
570 Lake, China: Journal of Environmental Sciences, v. 22(3), p. 328–337.
571 Yang, K., Lin, D., and Xing, B., 2009, Interactions of Humic Acid with Nanosized
572 Inorganic Oxides: Langmuir, v. 25, p. 3571-3576.
573 Zhang, H., and Banfield, J.F., 1998, Thermodynamic analysis of phase stability of
574 nanocrystalline titania: J. Mater. Chem., v. 8(9), p. 2073–2076.
575

576 **Figures**

577 Fig. 1: Mediterranean sapropels (see Tab. 1-3 for sample characteristics). (a, d, g): High-
578 magnification scanning transmission electron microscopy (STEM) images (high-
579 angle annular dark-field [HAADF] mode) showing brookite crystals (dotted circles).
580 (b, e, h): TEM Bright Field image of brookite crystals. Brookite occurs either as
581 single crystals (b) or in form of agglomerates (e, h). (c, f, i): FFT diffraction pattern
582 of crystals shown in (b, e, h) proving that brookite is the titania polymorph.

583

584 Fig. 2: Posidonia Shale of different thermal maturity (see vitrinite reflectance data at the
585 bottom, and Tab. 1-3 for sample characteristics). (a, d, g): High-magnification
586 scanning transmission electron microscopy (STEM) images (high-angle annular
587 dark-field [HAADF] mode) showing brookite crystals. (b, e, h): TEM Bright Field
588 images of brookite single crystals. (c, f, i): FFT diffraction pattern of crystals shown
589 in (b, e, h) proving that brookite is the titania polymorph. Zone-axis in 2i is [010].

590

591 Fig. 3: Bakken Shale (see Tab. 1-3 for sample characteristics). (a, d, g): High-
592 magnification scanning transmission electron microscopy (STEM) images (high-
593 angle annular dark-field [HAADF] mode) showing brookite crystals (dotted circles).
594 (b, e, h): TEM Bright Field images of brookite single crystals. (c, f, i): FFT
595 diffraction pattern of crystals shown in (b, e, h) proving that brookite is the titania
596 polymorph. Zone-axis in 3c is [2-13].

597

598 Fig. 4: Alum Shale (see Tab. 1-3 for sample characteristics). (a, d, g): High-magnification
599 scanning transmission electron microscopy (STEM) images (high-angle annular
600 dark-field [HAADF] mode) showing brookite and anatase crystals (dotted circles).

(b, e, h): TEM Bright Field images of an agglomerate of brookite crystals (e) and of anatase single crystals (b, h). (f, i): FFT diffraction pattern of crystals shown in (e, h) proving that brookite and anatase are the titania polymorphs. (c): HREM image of anatase.

Fig. 5: SAFOD sample #1856 (see Tab. 1, 2, and 4 for sample characteristics). (a): High-magnification scanning transmission electron microscopy (STEM) image (high-angle annular dark-field [HAADF] mode) showing a large agglomerate of anatase nano-crystals (dotted circle). (b): High-magnification scanning transmission electron microscopy (STEM) image (high-angle annular dark-field [HAADF] mode) showing anatase agglomerates (dotted circles). (c): FFT diffraction pattern of the anatase crystals. Zone-axis is [-110]. Wealden Shale sample #2953 (see Tab. 1, 2, and 4 for sample characteristics). (d): High-magnification scanning transmission electron microscopy (STEM) image (high-angle annular dark-field [HAADF] mode) showing a large anatase crystal (dotted circle). (e): High-magnification scanning transmission electron microscopy (STEM) image (high-angle annular dark-field [HAADF] mode) highlighting zonal fluid inclusions in the anatase crystal (filled by nitrogen gas). (f): Electron diffraction image of the large crystal shown in (a) proving that anatase is the titania polymorph. Zone-axis is [1-11].

Fig. 6: BSE images of a reservoir sandstone sample from an oil-water contact (see Tab. 1, 2, and 4 for sample characteristics) showing beginning rutile corrosion coupled to anatase formation. (a): rutile with corrosion features, (b): pore-filling anatase cement, (c): TEM Bright Field image of anatase agglomerate, (d): High-magnification scanning transmission electron microscopy (STEM) image (high-angle annular dark-

field [HAADF] mode) showing anatase agglomerate as in (c), (e) High-magnification scanning transmission electron microscopy (STEM) image (high-angle annular dark-field [HAADF] mode) showing anatase single crystals, (f) FFT electron diffraction pattern of single anatase crystal shown in (e). Zone in 6f is [100].

Fig. 7: Brookite and anatase occurrence either as single crystals or as agglomerate in dependence on TOC content and thermal maturity in the investigated samples. The grey field indicates the non-black shale samples. In this grey field, as it does not fit into the TOC/R_r plot, the anatase occurrence at the oil-water contact in the Siri oilfield is presented as single crystals or as agglomerates.

Fig. 8: Enthalpy of titania polymorphs as a function of surface area (redrawn after Navrotsky, 2004, basically after Ranade et al., 2002). Although the crystalline polymorph rutile is thermodynamically the most stable one, anatase and brookite are often only slightly metastable by only a few kilojoules per mole. Brookite has a surface enthalpy of approximately 1.0 J/m^2 which is higher than for anatase (0.4 J/m^2). Moreover, for titania particles with an surface area higher than around 4.000 m^2/mol (thus for smallest particles), anatase has the lowest enthalpy and can directly transform into brookite (Ranade et al. 2002). At a crossover size of about 30 nm anatase nanoparticles may directly transform into rutile (Zhang and Banfield 1998, Navrotsky 2003).

Fig. 9: Summarizing sketches about brookite and anatase formation in black shale (a) and at oil-water contacts (b).

652 **Tables**

653 Table 1: Origin of the investigation material.

654

655 Table 2: Thermal maturity (vitrinite reflectance, Rr), organic matter type and Rock Eval
656 data (HI, OI, Tmax), and TiO2 polymorph type of the investigation material. Origin
657 of data: (i) Mediteraanean sapropels: J. Möbius (Hamburg; pers. comm.); (ii) Alum
658 Shale (Schulz et al., 2015); (iii) Schöneck Formation (Schulz et al., 2002); (iv)
659 Bakken Shale (Kuhn et al., 2010); (v) Posidonia Shale (Bernard et al., 2012); (vi)
660 Wealden (Lüders, pers. comm.); (vii) SAFOD (Jansen et al., 2014); (viii) Heimdal
661 Formation (Mu et al., 2015).

662

663 Table 3: Indices of titania polymorphs and agglomeration in black shale.

664

665 Table 4: Indices of titania polymorphs and agglomeration in different environments.

666

Table 1: Origin of the investigation material

Sample No.	Name	Stratigraphy	Location	Well depth (m)
G014094	Mediterranean Sapropel S1	Holocene	Eastern Mediterranean Sea	0.27 m, at 3,090 m water depth
G014095	Mediterranean Sapropel S5	Pleistocene	Eastern Mediterranean Sea	2.70 m, at 2,788 m water depth
G014096	Mediterranean Sapropel S6	Pleistocene	Eastern Mediterranean Sea	4.12 m, at 2,788 m water depth
G011700	Alum Shale	Furongian (Upper Cambrian)	Southern Sweden	74.42
G011702	Alum Shale	Furongian (Upper Cambrian)	Southern Sweden	75.45
G011703	Alum Shale	Furongian (Upper Cambrian)	Southern Sweden	77.35
-	Schöneck Fm.	Oligocene	Upper Austria	1,384
G005270	Bakken Shale	Upp. Devonian-Low. Mississippian	Williston Basin (North Dakota, USA)	2,332
G005277	Bakken Shale	Upp. Devonian-Low. Mississippian	Williston Basin (North Dakota, USA)	2,344
G005298	Bakken Shale	Upp. Devonian-Low. Mississippian	Williston Basin (North Dakota, USA)	1,010
G007143	Posidonia Shale	Toarcian (Liassic)	Lower Saxony (Germany)	45.7
G007049	Posidonia Shale	Toarcian (Liassic)	Lower Saxony (Germany)	55.7
G007098	Posidonia Shale	Toarcian (Liassic)	Lower Saxony (Germany)	46.1
#2953	Wealden	Earliest Cretaceous	Lower Saxony (Germany)	926
#1856	SAFOD	?	USA	3,194
G012222	Heimdal Fm.	Miocene	Oil-water contact in sandstone, Danish North Sea	2,116, at 58 m water depth

Table 2:
Thermal maturity (vitrinite reflectance, R_r), organic matter type and Rock Eval data (HI, OI, Tmax), and TiO_2 polymorph type of the investigation material. Origin of data: (i) Mediteraanean sapropels: J. Möbius (Hamburg; pers. comm.); (ii) Alum Shale (Schulz et al., 2015); (iii) Schöneck Formation (Schulz et al., 2002); (iv) Bakken Shale (Kuhn et al., 2010); (v) Posidonia Shale (Bernard et al., 2012); (vi) Wealden (Lüders, pers. comm.); (vii) SAFOD (Janssen et al., 2014); (viii) Heimdal Formation (Mu et al., 2015).

Sample No.	**Name**	**R_r (%)**	**Total organic carbon (TOC, wt.%)**	**Organic matter type**	**Hydrogen index HI (mg HC/g TOC)**	**Oxygen index OI (mg CO_2/g TOC)**	**Tmax (°C)**	**TiO_2 polymorph**
G014094	Mediterranean Sapropel S1	~0.3	1.5-2.0	marine	n.d.	n.d.	n.d.	**Brookite**
G014095	Mediterranean Sapropel S5	~0.3	7.1-8.5	marine	n.d.	n.d.	n.d.	**Brookite**
G014096	Mediterranean Sapropel S6	~0.3	4.0-5.5	marine	n.d.	n.d.	n.d.	**Brookite**
G011700	Alum Shale	0.42	14.3	marine	518	2	424	*Anatase*
G011702	Alum Shale	0.42	n.d.	marine	n.d.	n.d.	n.d.	**Brookite**
G011703	Alum Shale	0.42	n.d.	marine	n.d.	n.d.	n.d.	*Anatase*
-	Schöneck Fm.	0.4	3.6	lacustrine	550	n.d.	430	**Brookite**
G005270	Bakken Shale	0.5	16.35	marine	468	7	427	**Brookite**
G005277	Bakken Shale	0.5	8.48	marine	221	15	427	**Brookite** + *Anatase*
G005298	Bakken Shale	0.4	8.25	marine	416	27	413	**Brookite**
G007143	Posidonia Shale	0.53	10.8	marine	617	15	430	**Brookite**
G007049	Posidonia Shale	0.88	11	marine	282	5	449	**Brookite**
G007098	Posidonia Shale	1.45	6.77	marine	83	7	468	**Brookite**
#2953	Wealden	1.6	3.3	terrestrial	29	16	532	*Anatase*
#1856	SAFOD	n.d.	n.d.	-	n.d.	n.d.	n.d.	*Anatase*
G012222	Heimdal Fm.	n.d.	n.d.	Oil-water contact	n.d.	n.d.	n.d.	*Anatase*

Table 3: Indices of titania polymorphs and agglomeration in black shale

Sample No.	Name	R_r (%)	Angle	calculated angle (°)	observed angle (°)	TiO_2 polymorph	Agglomerate (yes/no)
G014094	Med.Sapropel S1	~0.3	$\angle$ 110/311 $\angle$ 201/311	39.6 28	39.76 27.85	**Brookite**	n
G014095	Med. Sapropel S5	~0.3	$\angle$ 511/321 $\angle$ 511/2$\bar{1}$0	27.98 60.52	27.53 61.76	**Brookite**	y
G014096	Med. Sapropel S6	~0.3	$\angle$ 311/201 $\angle$ 311/101	29.32 38.70	28.9 41.0	**Brookite**	**y**
			$\angle$ 210/11$\bar{1}$ $\angle$ $\bar{1}$0$\bar{1}$/11$\bar{1}$	45.75 66.21	46.7 64.0	**Brookite**	**y**
G011700	Alum Shale	0.42	$\angle$ 013/011 $\angle$ 013/002	28.35 39.95	31.70 46.55	*Anatase*	n
G011702	Alum Shale	0.42	$\angle$ 310/111 $\angle$ 310/20$\bar{1}$	50.2 49.4	49 49	**Brookite**	y
G011703	Alum Shale	0.42	$\angle$ 123/121 $\angle$ 123/002	18.01 61.90	18.1 62	*Anatase*	n
-	Schöneck Fm.	0.4	$\angle$ 112/210 $\angle$ 112/$\bar{1}$02	63 38.91	63.3 38.3	**Brookite**	y
			$\angle$ 002/$\bar{1}\bar{1}$1 $\angle$ 002/111	47.64 47.64	48.3 48.3	**Brookite**	y
G005270	Bakken Shale	0.5	$\angle$ 201/1$\bar{1}$0 $\angle$ 201/111	67.01 43.10	71.0 43.0	**Brookite**	y
			$\angle$ 0$\bar{2}$ 1/1$\bar{1}$0 $\angle$ 0$\bar{2}$ 1/$\bar{1}\bar{1}\bar{1}$	40.57 28.70	40.0 27.9	**Brookite**	y
G005277	Bakken Shale	0.5	$\angle$ 311/201 $\angle$ 311/110	27.85 39.76	28.3 39.4	**Brookite**	n
			$\angle$ 105/011 $\angle$ 105/1$\bar{1}$4	70.71 28.50	69 28.3	*Anatase*	n
G005298	Bakken Shale	0.4	$\angle$ 111/$\bar{1}$01 $\angle$ 111/210	66.21 45.75	68.8 43.25	**Brookite**	n
			$\angle$ 131/210 $\angle$ 131/$\bar{1}$21	42.5 26.6	40.5 26	**Brookite**	n
			$\angle$ $\bar{1}$21/$\bar{3}$11 $\angle$ $\bar{3}$11/$\bar{2}$ $\bar{1}$0	39.07 71.80	39.64 72.40	**Brookite**	n
G007143	Posidonia Shale	0.53	$\angle$ 221/210 $\angle$ 111/011	30.76 33.02	31.0 33.7	**Brookite**	n
G007049	Posidonia Shale	0.88	$\angle$ 120/011 $\angle$ 120/11$\bar{1}$	48.88 44.28	46.8 45	**Brookite**	n
G007098	Posidonia Shale	1.45	$\angle$ 1$\bar{2}$ 0/1$\bar{1}$1 $\angle$ $\bar{1}\bar{2}$ 0/$\bar{2}$ $\bar{1}\bar{1}$	59.89 46.40	60.1 45.35	**Brookite**	n
			$\angle$ 102/$\bar{1}$01 $\angle$ 102/210	44.9 32.6	44.8 33.3	**Brookite**	n

Table 4: Indices of titania polymorphs and agglomeration in samples others than black shale

Sample No.	Name	R_r (%)	Angle	calculated angle (°)	observed angle (°)	TiO_2 polymorph	Agglomerate (yes/no)
#2953	Wealden	1.6	∠ 204/213 ∠ 204/0$\bar{1}$1 ∠ $\overline{222}$ /0$\bar{1}$1 ∠ $\overline{222}$ / $\bar{2}\,\bar{1}\,\bar{3}$	24.41 76.69 57.84 21.07	25.3 76.6 57.6 20.95	*Anatase*	*n*
#1856	SAFOD	n.d.	∠ 112/011 ∠ 112/101	41.07 41.07	41.64 40.94	*Anatase*	*y*
G012222	Heimdal Fm.	n.d.	∠ 013/011 ∠ 013/002 ∠ 022/013 ∠ 022/01$\bar{1}$ ∠ 00$\bar{4}$ /01$\bar{1}$ ∠ 00$\bar{4}$/0$\bar{1}\,\bar{3}$	28.35 39.95 28.33 43.40 68.30 39.95	28.3 40.5 29 44 67 38	*Anatase*	y + n

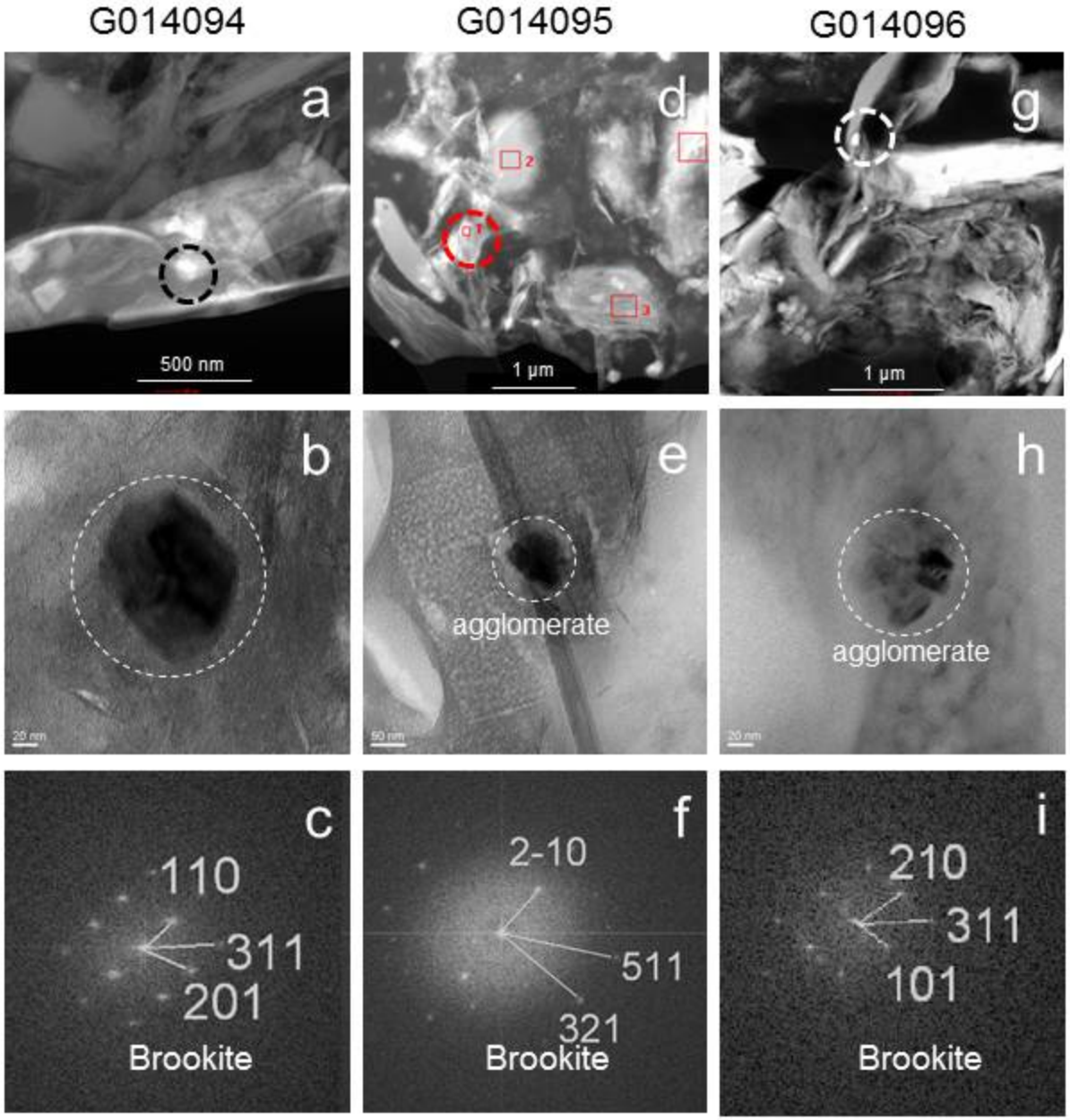
G014094
G014095
G014096
a
500 nm
d
1 µm
g
1 µm
b
e
agglomerate
h
agglomerate
c
110
311
201
Brookite
f
2-10
511
321
Brookite
i
210
311
101
Brookite

Fig. 1

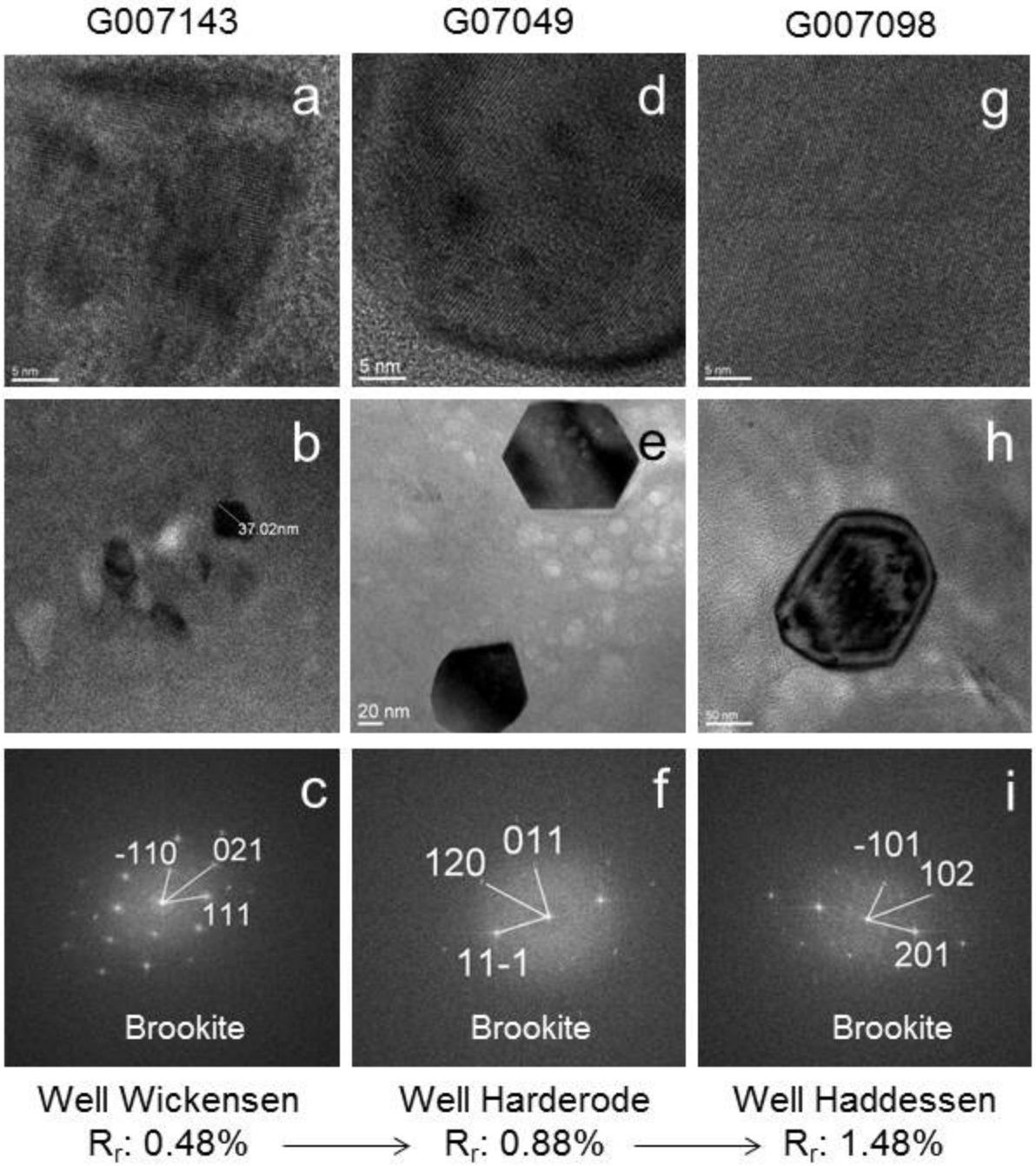
G007143
G07049
G007098
a
d
g
5 nm
5 nm
5 nm
b
e
h
37.02nm
20 nm
50 nm
c
f
i
-110
021
111
120
011
11-1
-101
102
201
Brookite
Brookite
Brookite
Well Wickensen
R$_r$: 0.48%
Well Harderode
R$_r$: 0.88%
Well Haddessen
R$_r$: 1.48%

Fig. 2

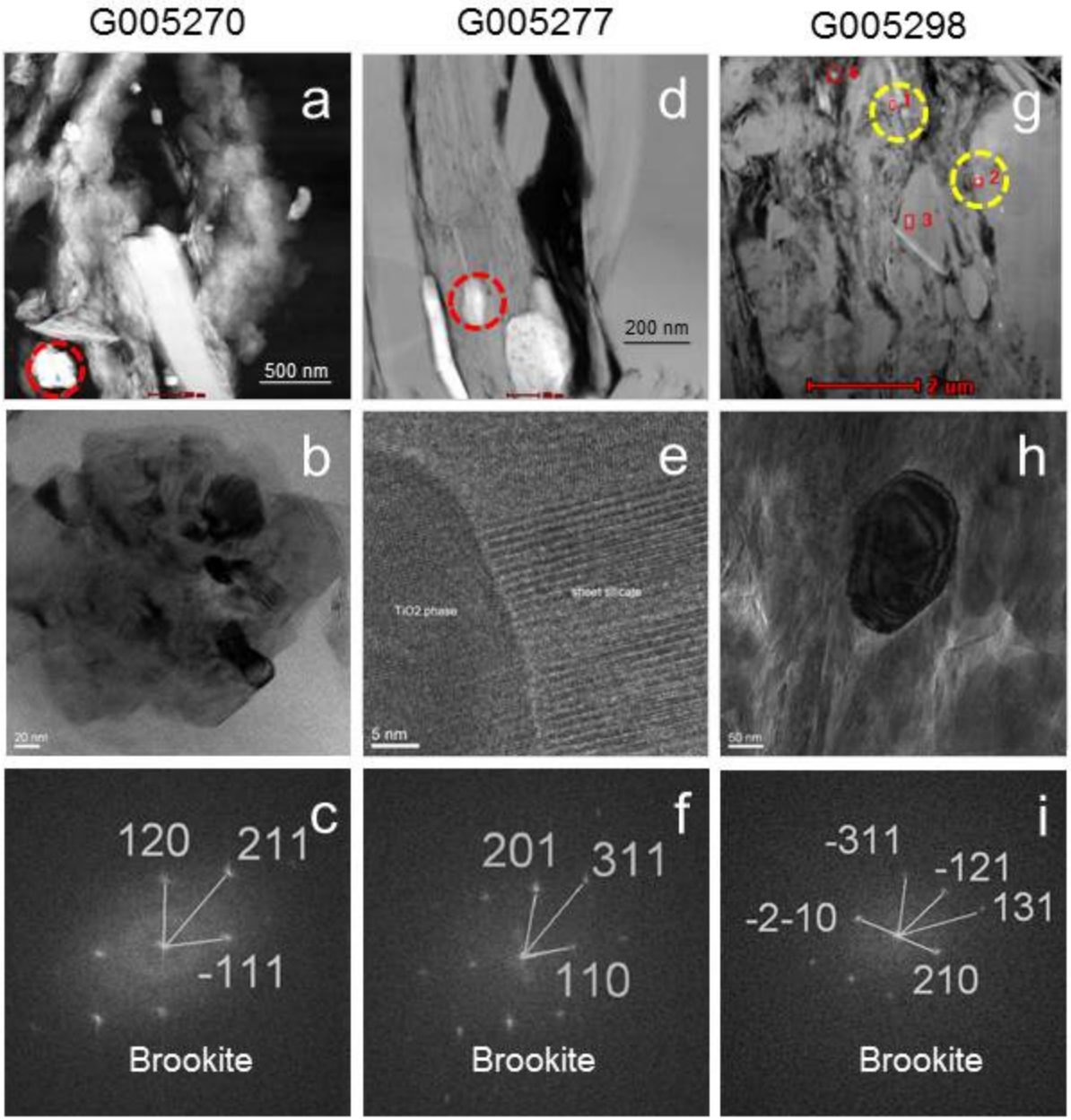
G005270
G005277
G005298
a
500 nm
d
200 nm
g
2 µm
b
20 nm
e
TiO2 phase
5 nm
h
50 nm
c
120
211
-111
Brookite
f
201
311
110
Brookite
i
-311
-121
-2-10
131
210
Brookite

Fig. 3

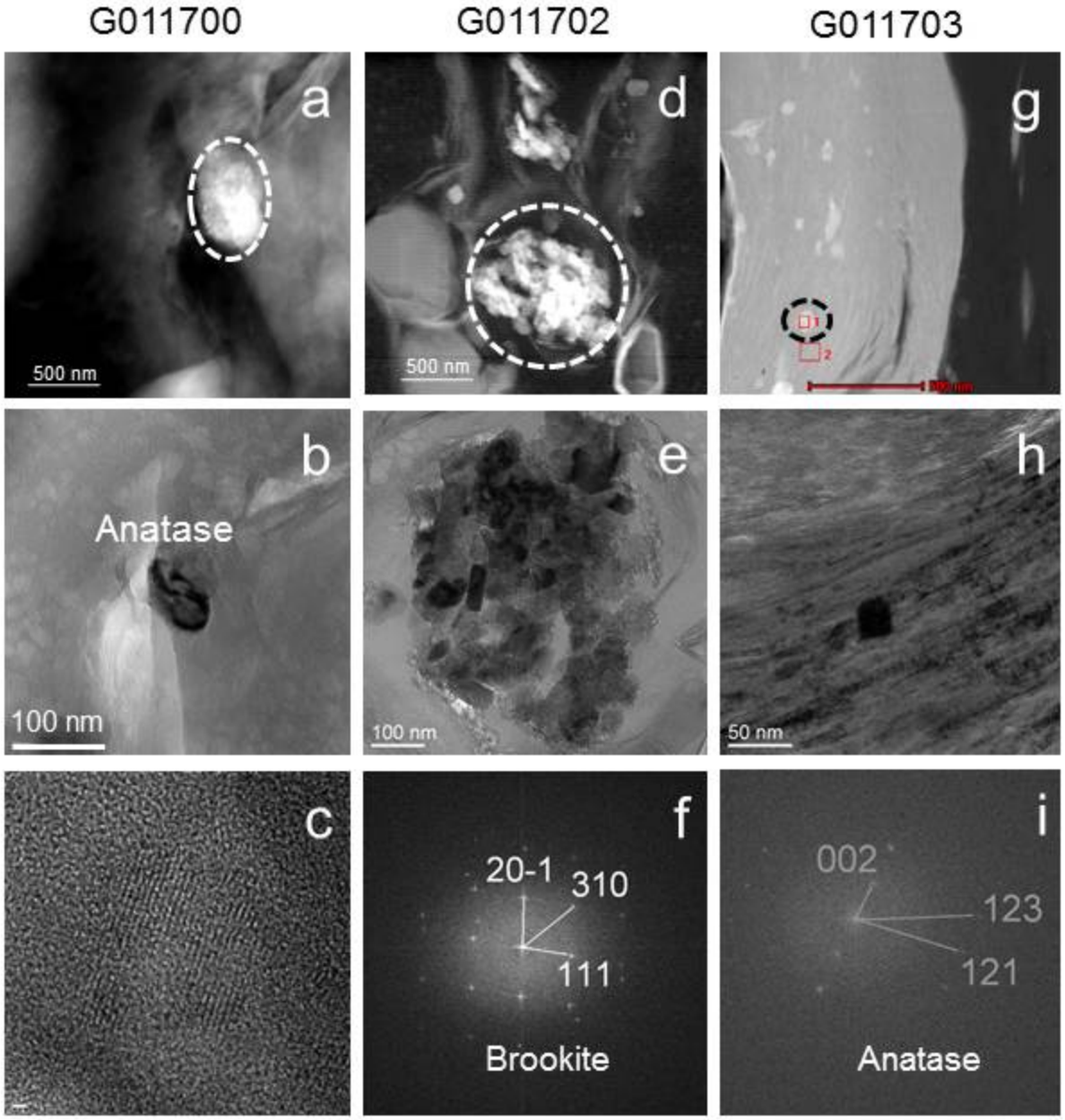
G011700
G011702
G011703
a
500 nm
d
500 nm
g
b
Anatase
100 nm
e
100 nm
h
50 nm
c
f
20-1
310
111
Brookite
i
002
123
121
Anatase

Fig. 4

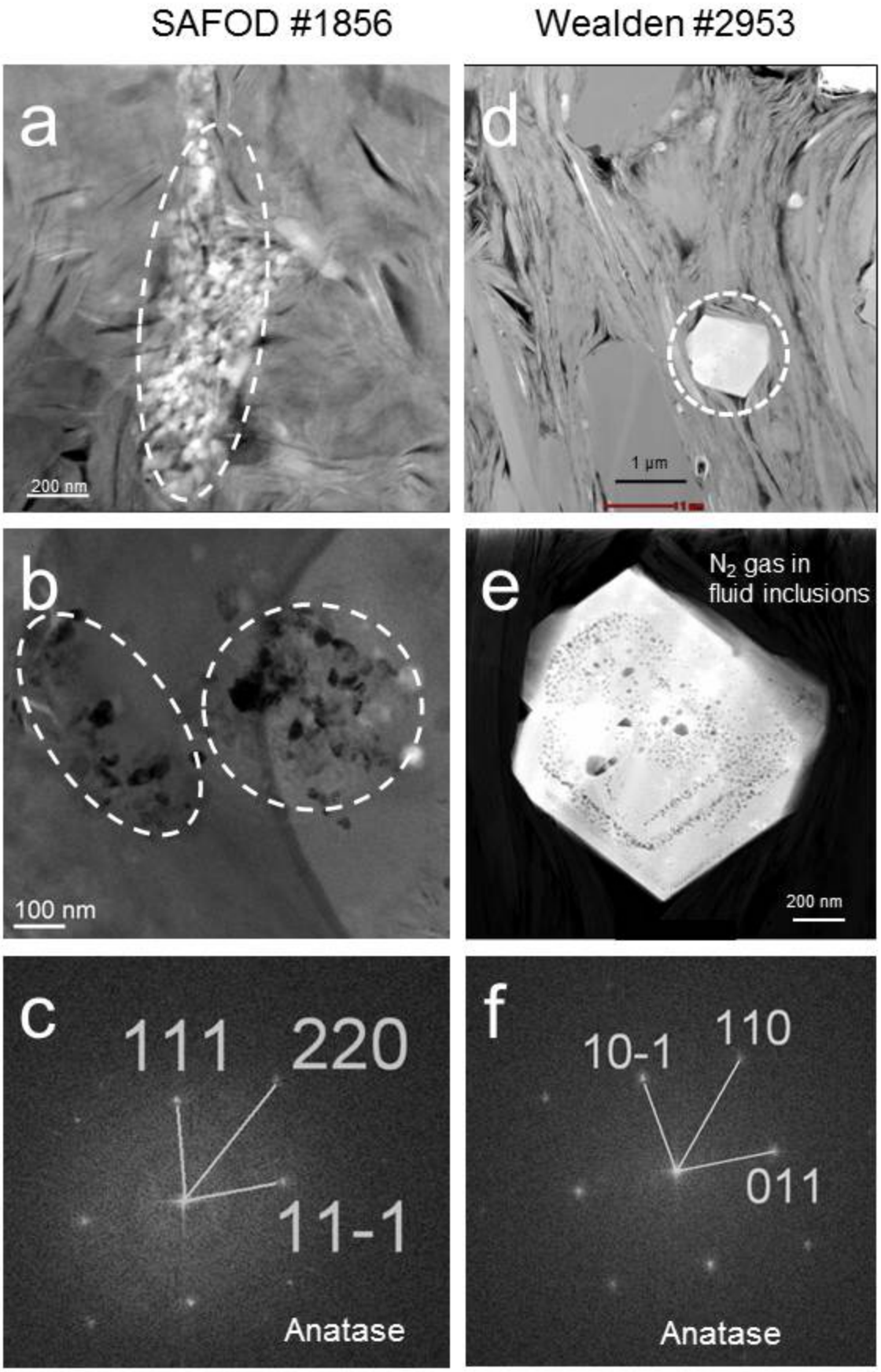
SAFOD #1856
Wealden #2953
a
200 nm
d
1 µm
b
100 nm
e
N_2 gas in
fluid inclusions
200 nm
c
111
220
11-1
Anatase
f
10-1
110
011
Anatase

Fig. 5

Oil-water contact - G012222

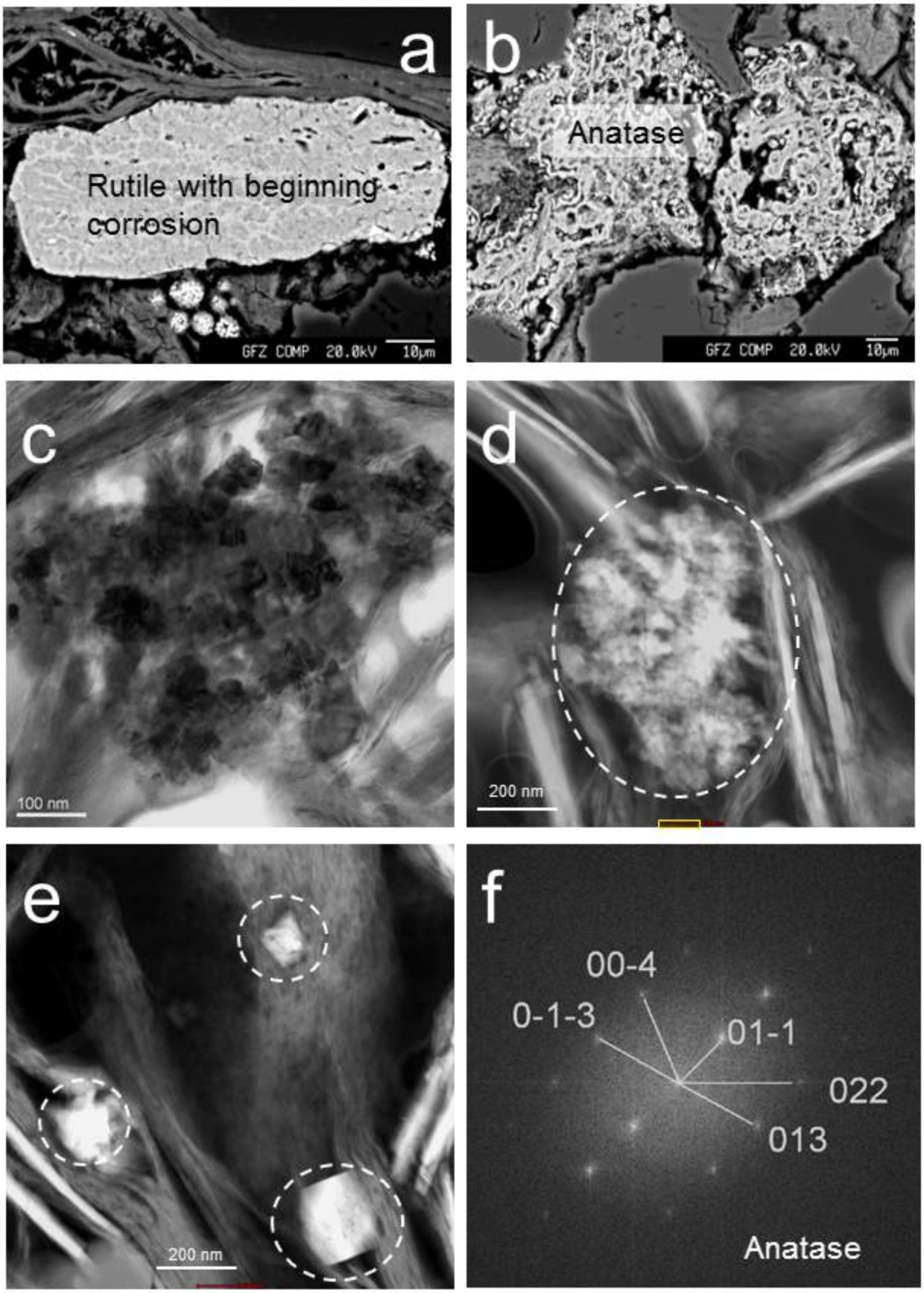

Fig. 6

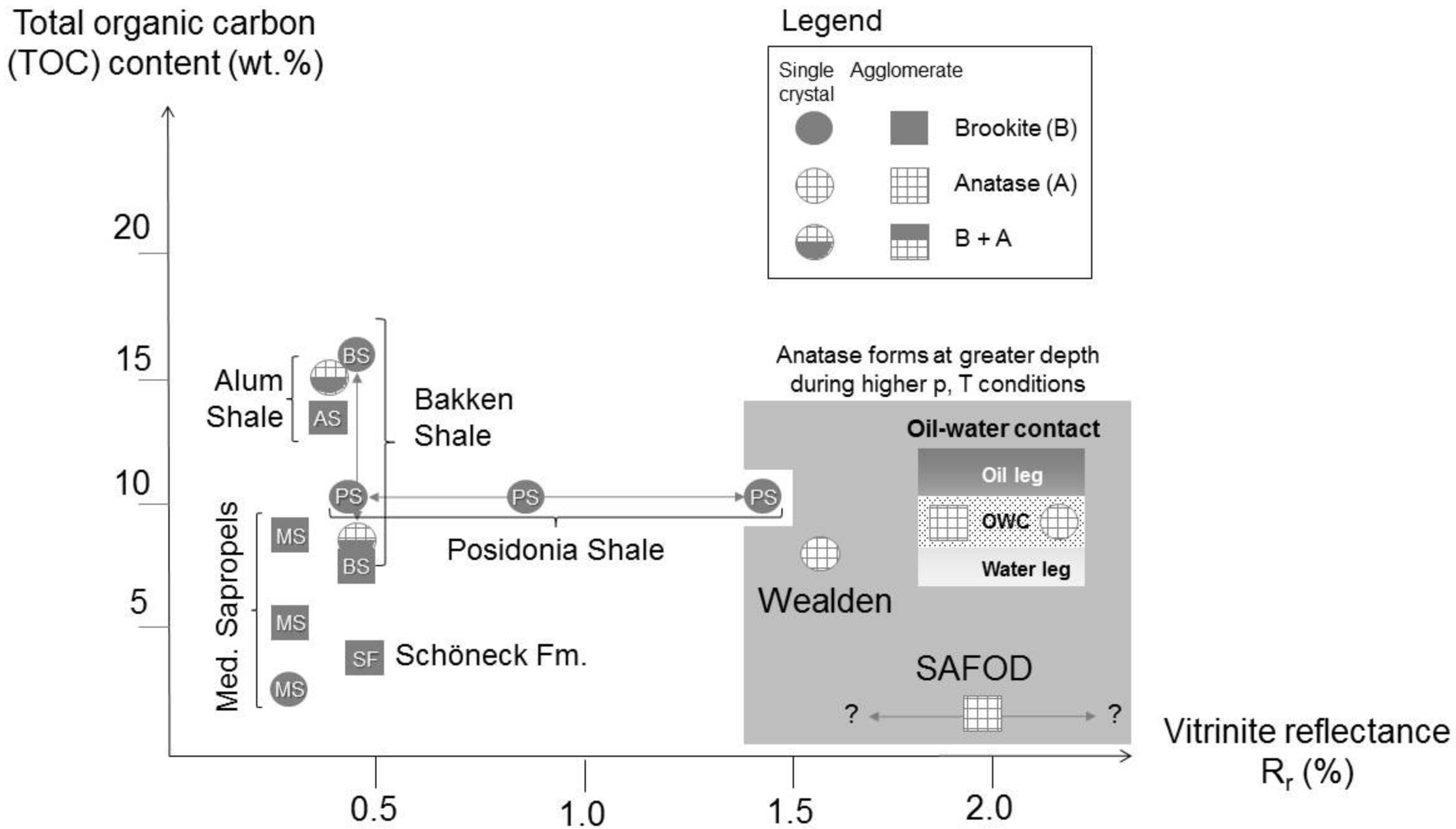
Total organic carbon
(TOC) content (wt.%)
20
15
10
5
Legend
Single crystal
Agglomerate
Brookite (B)
Anatase (A)
B + A
Anatase forms at greater depth
during higher p, T conditions
Oil-water contact
Oil leg
OWC
Water leg
Wealden
SAFOD
? ?
Alum Shale
AS
BS
Bakken Shale
PS
PS
PS
Posidonia Shale
BS
Med. Sapropels
MS
MS
MS
SF
Schöneck Fm.
0.5
1.0
1.5
2.0
Vitrinite reflectance
R_r (%)

Fig. 7

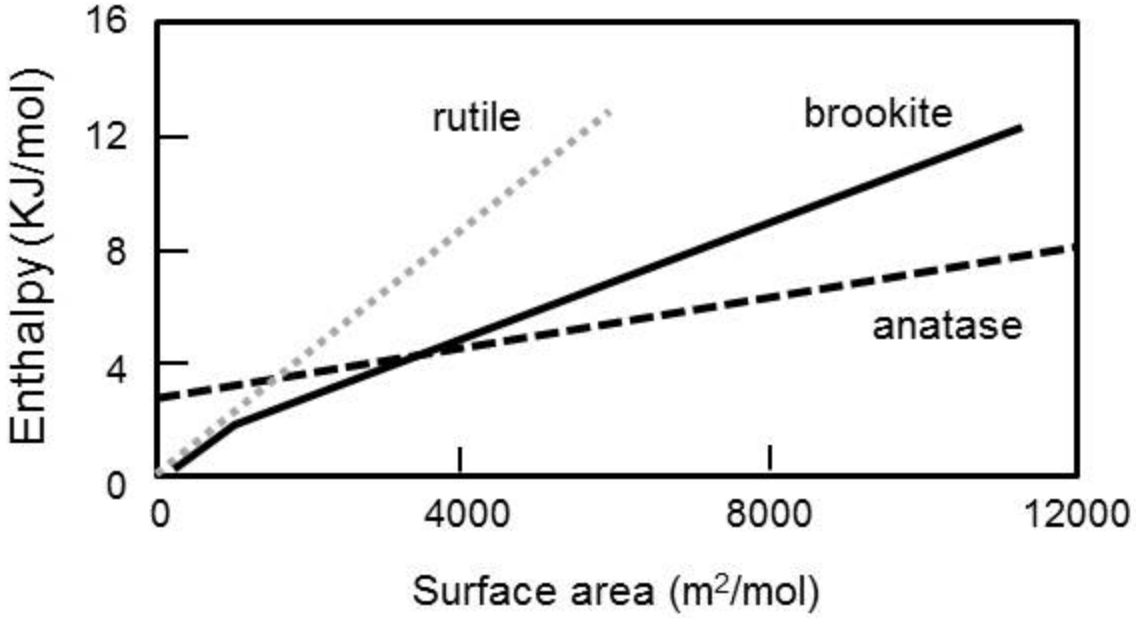
16
12
8
4
0
Enthalpy (KJ/mol)
rutile
brookite
anatase
0
4000
8000
12000
Surface area (m2/mol)

Fig. 8

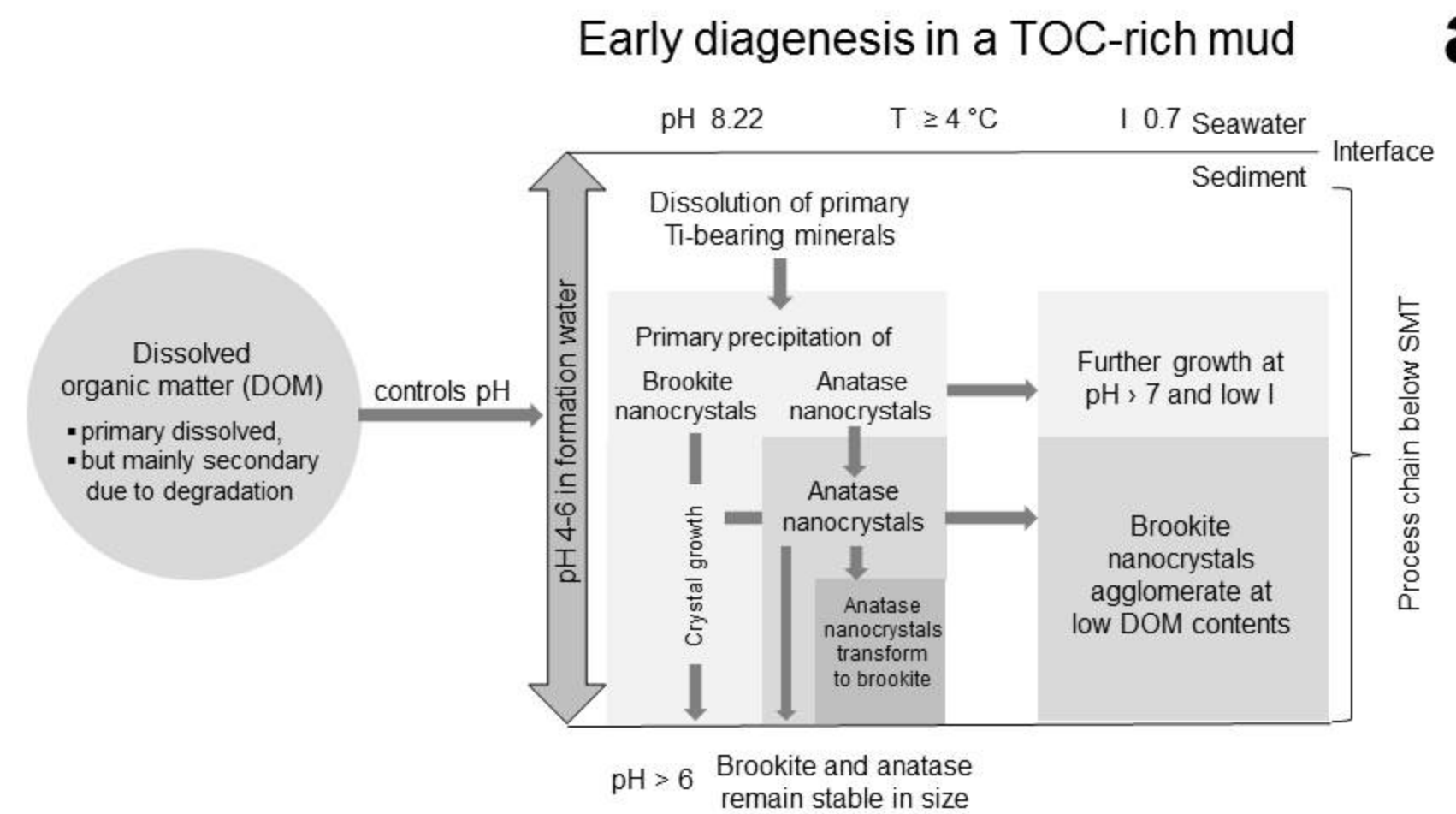
a
Early diagenesis in a TOC-rich mud
pH 8.22
T ≥ 4 °C
I 0.7 Seawater
Interface
Sediment
Dissolution of primary Ti-bearing minerals
Primary precipitation of
Brookite nanocrystals
Anatase nanocrystals
Further growth at pH › 7 and low I
Dissolved organic matter (DOM)
▪ primary dissolved,
▪ but mainly secondary due to degradation
controls pH
pH 4-6 in formation water
Crystal growth
Anatase nanocrystals
Anatase nanocrystals transform to brookite
Brookite nanocrystals agglomerate at low DOM contents
Process chain below SMT
pH › 6
Brookite and anatase remain stable in size
b
Processes at an oil-water contact
Dissolution of soluble oil components followed by anaerobic degradation
Oil Leg
Dissolved oil degradation products:
Formic acid, acetic acid, etc.
Naphthenic acid, etc.
Carbon dioxide
control pH
rel lower pH
↕
rel. higher pH
Dissolution of primary Ti-bearing minerals
Precipitation of anatase nanocrystals
Agglomeration of anatase nanocrystals inhibited by high contents of dissolved oil degradation products
Further growth of anatase nanocrystals
- oil/water ratio +
Oil-water transition zone
Water Leg
pH <3 to 7
T ≤ 80 °C
I > 0.7

Fig. 9